Cerebral, Facial, and Orbital Involvement in Erdheim-Chester Disease: CT and MR Imaging Findings[1]

Aurélie Drier, MD
Julien Haroche, MD, PhD
Julien Savatovsky, MD
Gaelle Godenèche, MD
Didier Dormont, MD
Jacques Chiras, MD
Zahir Amoura, MD
Fabrice Bonneville, MD, PhD

Purpose: To retrospectively review the brain magnetic resonance (MR) imaging and computed tomographic (CT) findings in patients with Erdheim-Chester disease (ECD).

Materials and Methods: The ethics committee required neither institutional review board approval nor informed patient consent for retrospective analyses of the patients' medical records and imaging data. The patients' medical files were retrospectively reviewed in accordance with human subject research protocols. Three neuroradiologists in consensus analyzed the signal intensity, location, size, number, and gadolinium uptake of lesions detected on brain MR images obtained in 33 patients with biopsy-proved ECD.

Results: Thirty patients had intracranial, facial bone, and/or orbital involvement, and three had normal neurologic imaging findings. The hypothalamic-pituitary axis was involved in 16 (53%) of the 30 patients, with six (20%) cases of micronodular or nodular masses of the infundibular stalk. Meningeal lesions were observed in seven (23%) patients. Three (10%) patients had bilateral symmetric T2 high signal intensity in the dentate nucleus areas, and five (17%) had multiple intraaxial enhancing masses. Striking intracranial periarterial infiltration was observed in three (10%) patients. Another patient (3%) had a lesion in the lumen of the superior sagittal sinus. Nine (30%) patients had orbital involvement. Twenty-four (80%) patients had osteosclerosis of the facial and/or skull bones. At least two anatomic sites were involved in two-thirds (n = 20) of the patients. Osteosclerosis of the facial bones associated with orbital masses and either meningeal or infundibular stalk masses was seen in eight (27%) patients.

Conclusion: Lesions of the brain, meninges, facial bones, and orbits are frequently observed and should be systematically sought on the brain MR and CT images obtained in patients with ECD, even if these patients are asymptomatic. Careful attention should be directed to the periarterial environment.

[1] From the Departments of Neuroradiology (A.D., D.D., J.C., F.B.) and Internal Medicine (J.H., Z.A.), Pitié-Salpêtrière Hospital, 47–83 Bd de l'Hôpital, 75013 Paris, France; Department of Neuroradiology, Rothschild Foundation, Paris, France (J.S.); Department of Neurology, Hôpital de la Milétrie, Poitiers, France (G.G.); and Department of Neuroradiology, Rangueil Hospital, Toulouse, France (F.B.). Received March 21, 2009; revision requested May 7; revision received September 4; accepted September 24; final version accepted November 2. **Address correspondence to** A.D. (e-mail: *aureliedrier@gmail.com*).

Erdheim-Chester disease (ECD) is a non–Langerhans cell form of histiocytosis that is characterized by xanthomatous infiltration of tissues by foamy histiocytes. ECD is an infrequent disease, with approximately 330 cases reported to date; it mainly affects patients in their 5th decade of life and has a slight male preponderance (1). ECD differs from Langerhans cell histiocytosis (LCH) in terms of the immunohistologic and microscopic characteristics of the respective histiocytes. It also differs from LCH clinically, mainly in terms of the severity of cardiovascular involvement, which is classically not seen in LCH. In addition, patients with ECD typically present with bone pain, and the disease is frequently characterized by bilateral symmetric long-bone osteosclerosis. About half of patients have extraskeletal manifestations, including xanthelasma, interstitial lung disease, retroperitoneal infiltration with periaortic fibrosis and perirenal and/or ureteral obstruction, renal failure, and exophthalmos.

Advances in Knowledge

- Intracranial periarterial lesions were present in 10% of patients with Erdheim-Chester disease (ECD).
- Osteosclerosis of facial bones associated with meningeal and orbital masses (17%) or with orbital and infundibular stalk masses (10%) was highly suggestive of a diagnosis of ECD.
- In cases of intracranial lesions of uncertain origin, the detection of an associated lesion of the facial bones or orbits on MR images may point to the diagnosis of ECD.
- Intracranial lesions in ECD, including intraaxial, meningeal, perivascular, and infundibular stalk lesions, are rarely isolated; patients with these lesions are almost always found at presentation to have either osteosclerosis of the sinus walls or orbital masses.

Neurologic symptoms are reported in about one-third of ECD cases (2). The most frequent central nervous system manifestations of ECD are diabetes insipidus, cerebellar syndromes, and symptoms that are related to extraaxial focal mass lesions and may lead to severe disability or death (3). The neurologic imaging features of the central nervous system involvement in ECD have been reported, generally in case reports (2,4–6); however, the literature lacks a systematic description of a substantial series of patients with ECD. Our purpose in this study was to better describe the cerebral, orbital, and facial involvements in ECD by retrospectively reviewing the brain magnetic resonance (MR) imaging and computed tomographic (CT) findings in patients with ECD.

Materials and Methods

This study was designed as a retrospective review. Neither institutional review board approval nor informed patient consent was required by the ethics committee of our institution (Pitié-Salpêtrière Hospital) for retrospective analyses of the patients' medical records and imaging data.

Patients and Criteria for Diagnosis

Thirty-three consecutive patients with a proved diagnosis of ECD were referred to the internal medicine department of our hospital between January 1996 and November 2007. All of these patients underwent at least one brain MR imaging examination; therefore, their data were included in this study. No patient's data were excluded, regardless of whether they were free of neurologic and/or ophthalmologic symptoms and whether their cerebral and/or facial MR and/or CT images were normal. Eleven patients in this series had been included in a previous work (7).

The diagnosis of ECD was established on the basis of widely accepted previously published histologic and skeletal criteria (1,8). Typical histologic findings are infiltration by foamy histiocytes nested among polymorphic granuloma, and fibrosis or xanthogranulomatosis with CD68-positive and CD1a-negative immunohistochemical staining, which is typical of ECD histiocytes. Typical skeletal findings are radiographically depicted bilateral symmetric cortical osteosclerosis of the diaphyseal and metaphyseal regions in the long bones and/or symmetric and abnormally strong labeling of the distal ends of the long bones of the legs and, in some cases, of the arms at technetium 99 bone scintigraphy. One patient had histopathologic findings consistent with both LCH and ECD patterns.

Fifteen of the 33 patients were found to have neurologic and/or ophthalmologic manifestations potentially

Implications for Patient Care

- In patients with ECD, cerebral MR imaging with gadolinium-based contrast material injection should be performed before starting treatment, even when no symptoms are present.
- In ECD, dedicated imaging of the orbits and sellar regions should be performed with thin sections owing to the relatively high frequency of lesions in these areas.
- Special attention should also be paid to the periarterial environment and venous compartment, as both asymptomatic and symptomatic lesions may manifest in these regions.

Published online
10.1148/radiol.10090320

Radiology 2010; 255:586–594

Abbreviations:
ECD = Erdheim-Chester disease
LCH = Langerhans cell histiocytosis

Author contributions:
Guarantors of integrity of entire study, A.D., J.C., F.B.; study concepts/study design or data acquisition or data analysis/interpretation, all authors; manuscript drafting or manuscript revision for important intellectual content, all authors; manuscript final version approval, all authors; literature research, A.D., J.H., J.S., F.B.; clinical studies, A.D., J.H., J.S., G.G., J.C., Z.A., F.B.; statistical analysis, A.D., J.H.; and manuscript editing, A.D., J.H., J.C., Z.A., F.B.

Authors stated no financial relationship to disclose.

related to central nervous system and/or orbital manifestations of ECD at presentation. These conditions were diabetes insipidus (n = 8), exophthalmos (n = 7), cerebellar ataxia (n = 4), seizures (n = 3), panhypopituitarism (n = 3), and/or papilledema with intracranial hypertension (n = 1). Eighteen (54%) patients were free of clinical symptoms potentially related to central nervous system or orbital involvement of ECD.

Imaging Examinations

At our institution, every patient with ECD undergoes a whole-body work-up, including at least fluorine 18–fluorodeoxyglucose positron emission tomography (PET), bone scintigraphy, cardiac MR imaging, thoracic and abdominal CT, and brain MR imaging. Therefore, all 33 patients with ECD, including those free of neurologic symptoms, underwent standard cerebral MR imaging, performed with an IRM 3T HDX or IRM 1.5T Excite unit (GE Medical Systems, Milwaukee, Wis), for evaluation of the extent of disease, which included, at least, T1-weighted (repetition time msec/echo time msec, 380/9) and T2-weighted (4650/102) spin-echo, fluid-attenuated inversion-recovery (repetition time msec/echo time msec/inversion time msec, 9000/114/2400), and gadoterate meglumine (Dotarem; Guerbet, Aulnay-sous-bois, France) enhanced T1-weighted (380/9) sequences. Additional dedicated sequences were performed according to specific clinical indications and/or immediate analysis of the images. Thus, 20 patients underwent dedicated MR imaging of the hypothalamic-pituitary axis, which involved the acquisition of 3-mm-thick contiguous coronal T1-weighted (380/9) and T2-weighted (4650/102) spin-echo images and coronal gadolinium-enhanced T1-weighted images (380/9).

Examination of the orbits was performed in 19 patients by using axial thin-section fat-suppressed gadolinium-enhanced T1-weighted MR images (380/9) and coronal T2-weighted images (4650/102). Dedicated CT of the sinuses was performed in 18 patients with a 16-section CT scanner (Somatom Sensation 16; Siemens, Erlangen, Germany) by using a section thickness of 0.75 mm, a tube current of 100 mAs, and a tube voltage of 120 kV. Fluorine 18–fluorodeoxyglucose PET scans were acquired by using a Gemini dual PET/CT scanner (Philips GLX Systems, Cleveland, Ohio), which is a combination of a helical 16-section CT scanner and a three-dimensional PET scanner. The imaging examinations performed, organs of interest assessed, and numbers of patients examined with specific imaging modalities in this study are summarized in Table 1.

Image Analysis

The MR and CT images were retrospectively reviewed in consensus by three neuroradiologists (A.D., J.S., F.B.; 3, 5, and 10 years experience in neuroradiology, respectively). The following lesion characteristics were analyzed: signal intensity on T1- and T2-weighted MR images, gadolinium uptake, number, location (hypothalamus, stalk, anterior and posterior pituitary lobes, meninges, dentate nucleus area, parenchymal region, perivascular region, orbits, facial and skull bones), and size (micronodular lesions < 3 mm in diameter, nodular lesions between 3 and 10 mm in diameter, and mass lesions > 10 mm in diameter).

Qualitative assessment of facial and skull bone involvement was performed by using both MR and CT images, when available. Characteristic areas of osteosclerosis were sought on CT images, and these appeared as thickened bone with low signal intensity on T1- and T2-weighted MR images. Data from fluorine 18–fluorodeoxyglucose PET were not assessed in the present study. However, in one patient, who had multiple ECD lesions, this examination first depicted unusual hypermetabolism in the superior sagittal sinus that was subsequently identified as an ECD lesion on brain MR images.

Table 1

Imaging Examinations, Organs Assessed, and Numbers of Patients

Imaging Examination	No. of Patients (n = 33)
Brain MR	33 (100)
Dedicated hypothalamic-pituitary axis MR	20 (61)
Dedicated orbit MR	19 (58)
Sinus CT	18 (54)

Note.—Numbers in parentheses are percentages.

Results

Of the 33 patients with ECD, 30 (90%) had abnormal neurologic imaging findings and three had normal MR and CT images. The 30 patients (mean age, 57 years; age range, 16–78 years) with abnormal examination results, which served as the basis for this study, were 20 male subjects (mean age, 54 years; age range, 16–74 years) and 10 female subjects (mean age, 57 years; age range, 18–78 years). The abnormal findings depicted on the cerebral MR and paranasal sinus CT images obtained in the 30 patients are summarized in Table 2.

Table 2

Cerebral, Facial, and Orbital Involvement in Patients with Abnormal Imaging Findings

Lesion Location and Type	No. of Patients (n = 30)
Hypothalamic-pituitary axis	16 (53)
Infundibular stalk	6 (20)
Absent bright spot in posterior pituitary lobe*	14 (47)
Meninges	7 (23)
Single dural mass	2 (7)
Multiple dural masses	2 (7)
Diffuse pachymeningeal thickening	3 (10)
Brain	6 (20)
High signal intensity in dentate nucleus area†	3 (10)
Intraaxial enhancing masses	5 (17)
Periarterial infiltration	3 (10)
Venous sinus lesion	1 (3)
Orbits	9 (30)
Bilateral intraconal lesions	6 (20)
Unilateral intraconal lesion	2 (7)
Extraconal lesion	1 (3)
Facial and skull bones	24 (80)
Maxillary and sphenoid sinuses	14 (47)
Ethmoidal or frontal sinuses	5 (17)
Cranial vault	8 (27)

Note.—Numbers in parentheses are percentages.

* T1-weighted MR imaging finding.

† T2-weighted MR imaging finding.

Hypothalamic-Pituitary Axis Involvement

The hypothalamic-pituitary axis was the most frequent site involved, with the high signal intensity of the posterior pituitary lobe normally seen on T1-weighted MR images being absent in 14 (47%) of the 30 patients. Notably, three (19%) of these 16 patients had panhypopituitarism, and eight (50%) were found to have diabetes insipidus at presentation. Six (20%) of the eight patients with diabetes insipidus had a single micronodular or nodular infundibular stalk mass up to 18 mm in diameter, with homogeneous intense enhancement after gadolinium-based contrast material administration (Fig 1). One of these lesions extended to the hypothalamus.

Meningeal Lesions

Meningeal lesions were observed in seven (23%) of the 30 patients. Four of these patients had meningioma-like mass lesions: a single dural mass in two patients and multiple dural masses (Fig 2a) in two others. Three patients were found to have diffuse pachymeningeal thickening at presentation, and one of these patients had focal masses superimposed on the pachymeningeal thickening (Fig 2). The meningeal lesions had an iso- or hypointense signal on T2-weighted images, an isointense signal on T1-weighted images, and homogeneous intense enhancement on gadolinium-enhanced T1-weighted images. Of the seven patients with meningeal lesions, only one (14%), who had chronic pachymeningitis, had intracranial hypertension syndrome that required ventriculoatrial shunt placement.

Intraaxial Lesions

In five (17%) of the 30 patients, we observed multiple enhancing intraaxial focal masses, with each patient harboring one to 16 lesions. These intraaxial mass lesions were supratentorial in four patients, each of whom harbored between one and 14 supratentorial masses ranging from 4 to 46 mm in diameter. Three patients had infratentorial confluent infratentorial nodules less than 10 mm in diameter. The intraaxial lesions typically had an isointense signal on T1-weighted images, an iso- or hypointense signal on T2-weighted images, and intense homogeneous enhancement on gadolinium-enhanced T1-weighted images. Three of the five patients with multiple intraaxial enhancing masses had neurologic focal signs and/or seizures.

Three (10%) of the 30 patients had bilateral symmetric high signal intensity in the dentate nucleus areas on T2-weighted MR images and corresponding low signal intensity on T1-weighted images (Fig 3a). These three patients were found to have cerebellar ataxia at presentation.

Figure 1

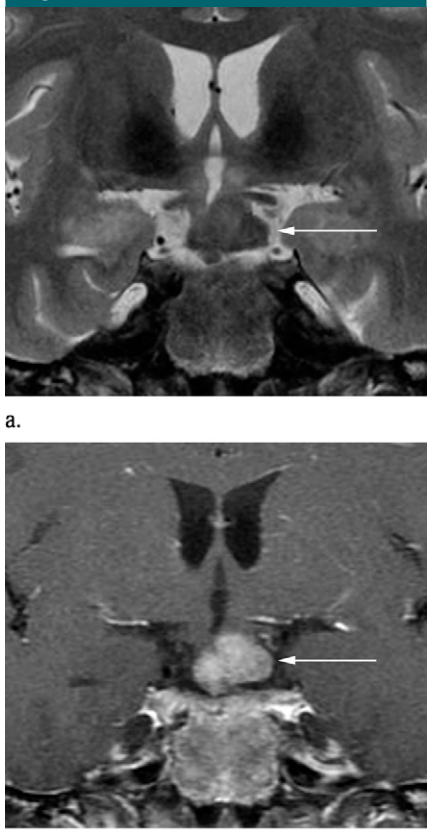

a.

b.

Figure 1: Coronal **(a)** T2-weighted (4650/102) and **(b)** T1-weighted gadolinium-enhanced (380/9) MR images in 30-year-old man with diabetes insipidus show nodular mass of infundibular stalk (arrow), with homogeneous intense enhancement after gadolinium-based contrast material administration (**b**).

Vascular Involvement

Intracranial periarterial enhancing abnormalities were observed in three (10%) of the 30 patients. One patient had a stenotic circumferential lesion of the basilar artery associated with multiple strokes in the vertebrobasilar territory. Another patient was free of neurologic symptoms but had a mass lesion encasing the left intracranial vertebral artery (Fig 4). The third patient, also free of neurologic symptoms, was

Figure 2

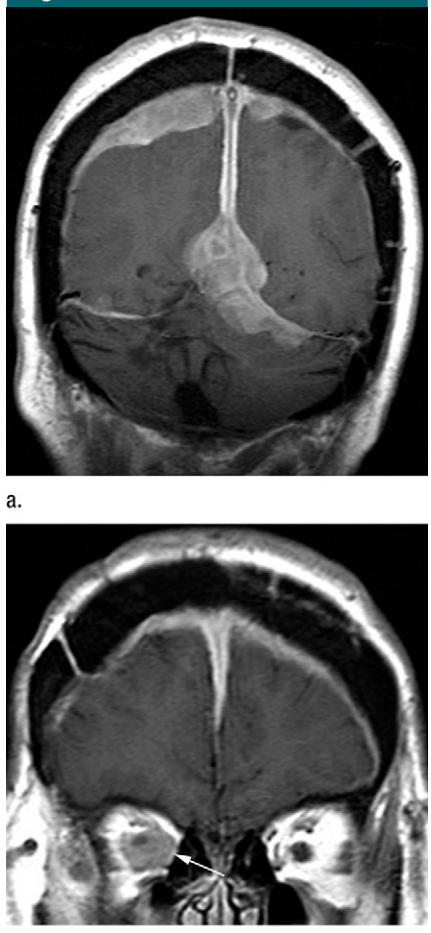

a.

b.

Figure 2: Coronal T1-weighted gadolinium-enhanced MR images (380/9) in 62-year-old woman with headaches show **(a)** multiple enhancing dural masses associated with diffuse enhancing dural thickening and diffuse skull bone thickening, in addition to **(b)** diffuse linear dural thickening and enhancement, diffuse skull bone thickening, and enhancing retro-ocular mass (arrow).

Figure 3

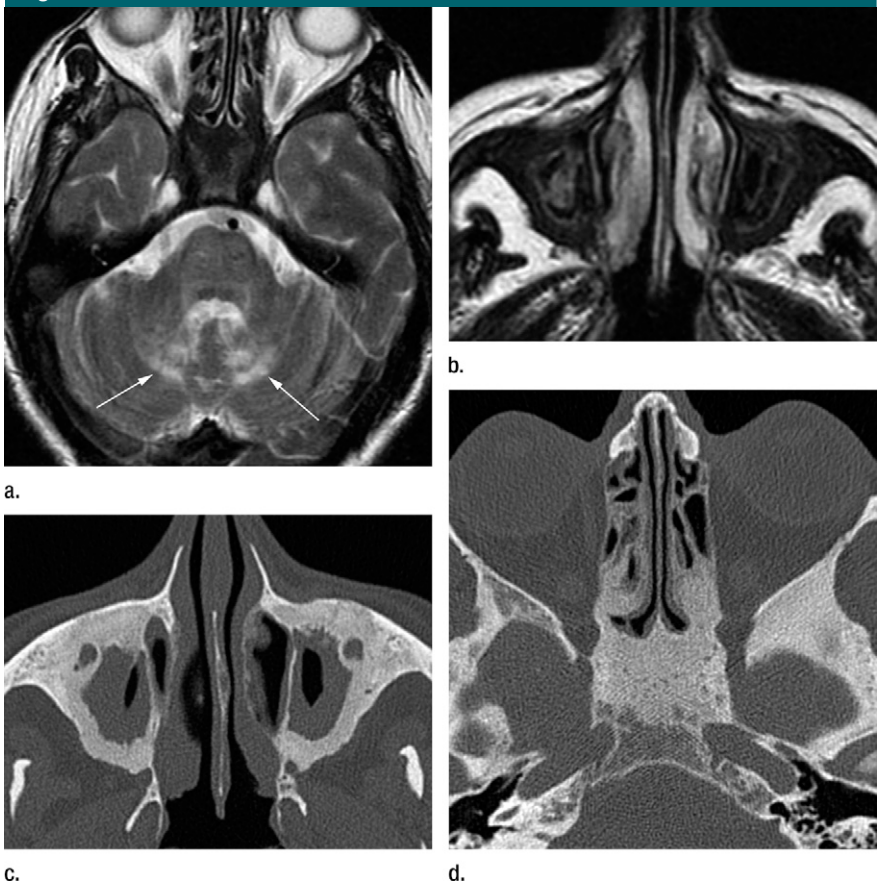

Figure 3: Axial images in 44-year-old man with cerebellar ataxia. **(a)** T2-weighted MR image (4650/102) shows symmetric hyperintense signal in peridentate regions (arrows) and osteosclerosis with low signal intensity filling the sphenoid sinus. **(b)** T2-weighted MR image (4650/102) shows bilateral maxillary sinus wall thickening with low signal intensity. Corresponding CT scans show **(c)** bilateral osteosclerosis and **(d)** osteosclerosis encompassing the sphenoid sinus and ethmoidal cells.

Figure 4

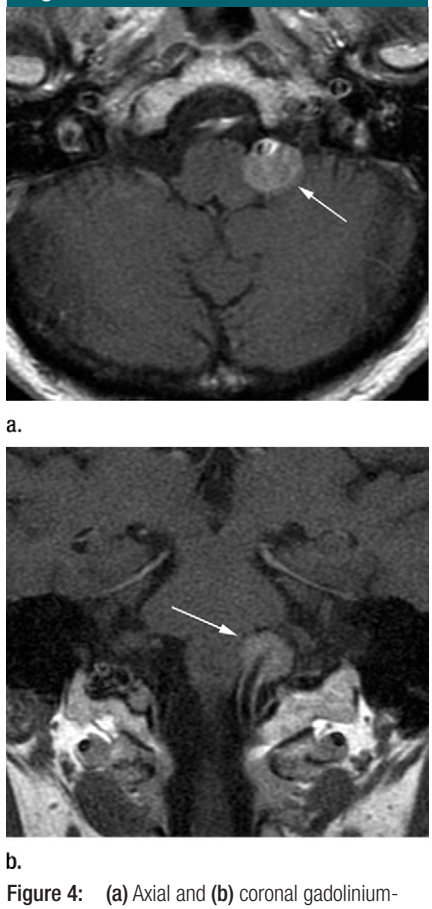

Figure 4: **(a)** Axial and **(b)** coronal gadolinium-enhanced T1-weighted MR images (380/9) in 63-year-old woman with ECD and no neurologic symptoms show encasement of the left vertebral artery by a homogeneously enhancing mass (arrow).

found at presentation to have bilateral intracavernous pericarotid infiltration contiguous with lesions surrounding both cervical internal carotid arteries (Fig 5).

One patient had a lesion in the lumen of the superior sagittal sinus but was clinically asymptomatic. This lesion had signal intensity and gadolinium enhancement on MR images and hypermetabolism on fluorine 18–fluorodeoxyglucose PET images that were similar to those of associated typical bilateral intraorbital lesions (Fig 6).

Orbital Involvement

Nine (30%) of the 30 patients had orbital involvement. Six of these patients were found to have bilateral intraconal masses at presentation. Among them, two patients had large masses extending to the extraconal space. Two other patients had unilateral intraconal masses. These orbital lesions had mainly a hypointense signal on both T1- and T2-weighted images and intense enhancement on gadolinium-enhanced T1-weighted images (Figs 6, 7). One patient with orbital involvement was found at presentation to have expansive bilateral ethmoidal mucoceles resulting in a major mass effect on the lamina papyracea. Seven of the nine patients with orbital involvement at MR and CT imaging were clinically found to have exophthalmos.

Sinus and Skull Involvement

Twenty-four (80%) of the 30 patients had facial and/or skull bone thickening. Fourteen of these patients had bilateral maxillary and sphenoid sinus wall osteosclerosis with a hypointense signal on T1- and T2-weighted MR images (Fig 3), and five had bilateral ethmoidal cell wall osteosclerosis (Fig 3d). Although 80% of the patients had sinus abnormalities at MR and CT imaging, only three (12%) of these 24 patients had clinical symptoms of sinusitis. For two of them, the histologic proof of ECD was found at sinus biopsy. Eight patients had osteosclerosis with diffuse thickening of the skull bone vault (Fig 2).

Figure 5

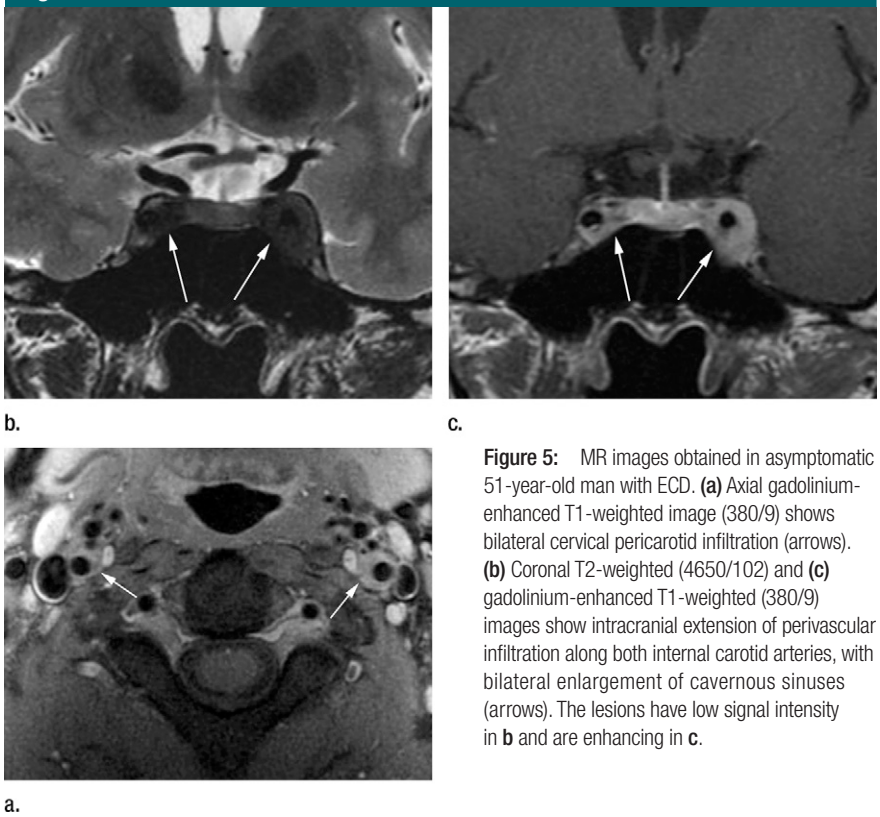

Figure 5: MR images obtained in asymptomatic 51-year-old man with ECD. **(a)** Axial gadolinium-enhanced T1-weighted image (380/9) shows bilateral cervical pericarotid infiltration (arrows). **(b)** Coronal T2-weighted (4650/102) and **(c)** gadolinium-enhanced T1-weighted (380/9) images show intracranial extension of perivascular infiltration along both internal carotid arteries, with bilateral enlargement of cavernous sinuses (arrows). The lesions have low signal intensity in **b** and are enhancing in **c**.

Frequent Associations with ECD Lesions

The neurologic images obtained in two-thirds (n = 20) of the 30 patients showed simultaneous involvement of two different anatomic sites. In eight (27%) of 30 cases, osteosclerosis of the facial bones was associated with orbital masses, and in seven (23%) cases, it was associated with a dural lesion. Each of five (17%) of the 30 patients was found at presentation to have osteosclerosis of the facial bones, meningeal masses, and orbital masses. Three (10%) patients each were found to have osteosclerosis of the facial bones, orbital masses, and infundibular stalk masses at presentation. In addition, intracranial lesions in ECD (ie, intraaxial, meningeal, perivascular, or infundibular stalk lesions) were never isolated, as all patients with such lesions were also found to have osteosclerosis of the sinus walls or orbital masses at presentation.

Discussion

Herein we report the MR and CT imaging features of intracranial, orbital, and facial involvement in a retrospective, single-center series of 33 patients with ECD, with emphasis on rarely described intracranial periarterial and intravenous lesions. Although a single case of peripheral fibrosis of the extracranial portion of the internal carotid artery at high-spatial-resolution MR imaging was reported once in a patient with ECD (9), to our knowledge, perivascular lesions of the intracranial carotid artery have not been previously reported. Perivascular infiltration and periaortic fibrosis are among the most frequent cardiovascular lesions in ECD, and they often worsen the prognosis for patients with this disease (9). Intracranial periarterial or intravenous infiltrations are exceedingly rare, but they may be overlooked because they can be asymptomatic. These infiltrations should be detected before catastrophic symptoms related to stroke develop. One patient in the current study had bilateral cervical internal pericarotid infiltration with low signal intensity on T2-weighted images, and the infiltration extended intracranially along both internal carotid arteries and enlarged the cavernous sinuses bilaterally. These lesions were asymptomatic, and the patient had no neurologic symptoms. Neither stroke nor cranial nerve palsy symptoms were observed clinically.

We identified another case without symptoms—that of an intracranial mass encasing the vertebral artery in a patient with typical lesions of the pituitary stalk and both orbits. Only one of three patients with mass lesions enveloping intracranial arteries was symptomatic. In this case, like two other cases reported in the literature (10,11), a mass that was encasing an artery of the vertebrobasilar system was discovered at examination for a stroke. These results justify the systematic search for intracranial periarterial lesions among patients with ECD.

Lesions in venous sinuses are extremely rare as well. To our knowledge, only one case of a mass in the torcula with thrombosis of both transverse sinuses has been described (12). In our series, one asymptomatic patient had a nonocclusive lesion in the superior sagittal sinus, consistent with a specific ECD involvement. Because it had MR imaging and PET features similar to those of several other scattered lesions with histologic and immunohistochemical proof of ECD based on biopsy findings in this patient, despite the lack of direct proof of the nature of this perivenous lesion in vivo, it almost certainly corresponded to an ECD location.

Long-bone involvement is an almost constant finding in ECD, and there are just a few case reports of axial skeleton involvement in the literature (7,13). Bone involvement is characterized at conventional radiography by symmetric bilateral osteosclerosis of the metaphysis and diaphysis of the long bones, sparing the axial skeleton, as well as the hands and feet (7). Facial and skull bone lesions also have been rarely

Figure 6

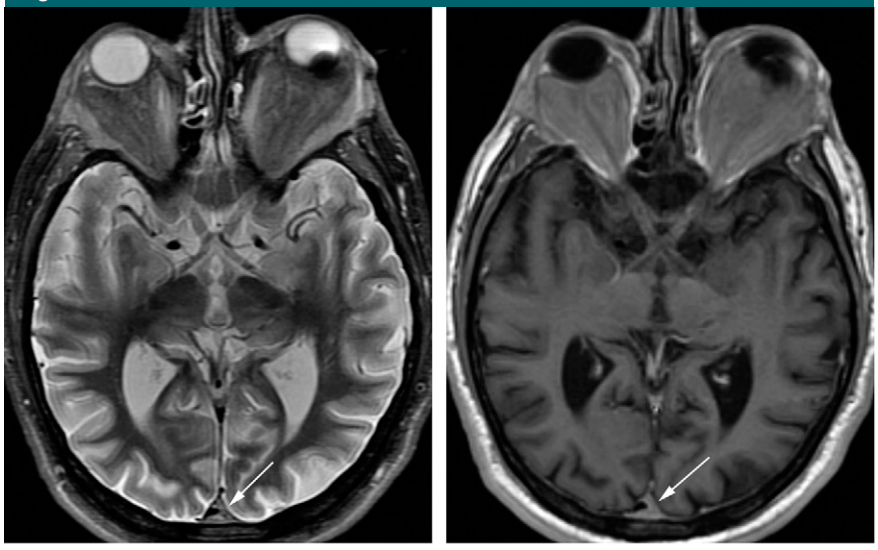

a. b.

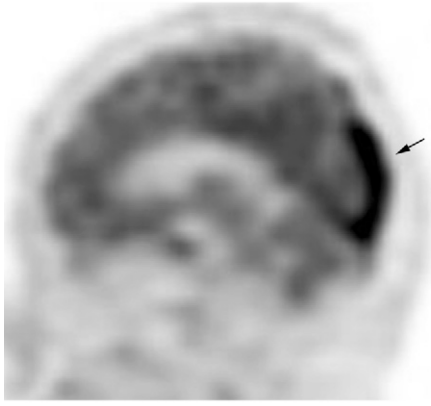

c.

Figure 6: Images in 62-year-old man with exophthalmos. Axial **(a)** T2-weighted short inversion time inversion-recovery (3500/60/150) and **(b)** gadolinium-enhanced T1-weighted (380/9) MR images show lesion in lumen of superior sagittal sinus (arrow), with similar low signal intensity (at T2-weighted imaging) and enhancement (at gadolinium-enhanced imaging) compared with typical bilateral intraorbital masses. **(c)** Sagittal PET scan shows fixation (arrow) in superior sagittal sinus.

Figure 7

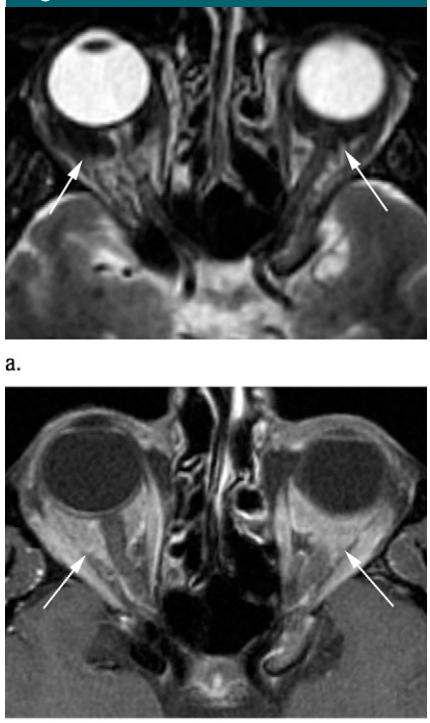

a. b.

Figure 7: Axial **(a)** T2-weighted (4650/102) and **(b)** gadolinium-enhanced fat-suppressed T1-weighted (380/9) MR images in 40-year-old man with exophthalmos show bilateral retro-ocular intraconal infiltration (arrows). Lesions have low signal intensity in **a** and are enhancing in **b**.

reported (14). In our series, however, osteosclerosis of the maxillary and sphenoid sinus walls was frequent and was characterized by thickened bone on CT images and a hypointense signal on T1- and T2-weighted MR images. We also observed thickening of the skull bones with similar imaging features in many cases. Although skull involvement is a well-established pattern of LCH, it is less frequently described in association with ECD (15). However, the features of the ECD-associated skull lesions in our series were different from those of LCH. In LCH, these bone lesions appear as well-circumscribed lytic lesions, while in ECD, they result in osteosclerosis and bone thickening. However, according to the literature, facial and skull bone lesions in ECD may show two distinct patterns: symmetric osteosclerosis of the facial bones, as observed in all of our cases, and, rarely, focal pseudotumoral lesions (7). These pseudotumoral lesions have been described with variable degrees of osteolysis, cortical destruction, and soft-tissue mass (7,16), which may resemble lytic LCH lesions.

In our study, about half the patients had hypothalamic-pituitary axis abnormalities; however, the true prevalence of these lesions may be even greater since dedicated sellar examinations were not universally performed. The high signal intensity of the posterior pituitary lobe normally seen on T1-weighted MR images was lacking in many patients; this was often associated with a pituitary stalk and/or a hypothalamic lesion. Absence of the posterior pituitary lobe "bright spot" may be important in these patients: Two patients who were found to have central diabetes insipidus at presentation in our series lacked a T1 bright spot in the posterior pituitary lobe, but they did not harbor a visible granulomatous lesion on the hypothalamus-hypophyseal axis.

In ECD, pachymeningeal thickening or well-circumscribed meningioma-like dural mass lesions have been reported often at the falx cerebri, cerebellar tentorium, or sellar region and more rarely at the spinal level (4,17,18). In previous studies, as in our series, dural masses have been asymptomatic when they were small and symptomatic when they were large enough to compress adjacent

neural structures (19). At MR imaging, these well-defined masses often had low signal intensity on T2-weighted images, suggestive of the diagnosis. With ECD, the uptake of gadolinium in dural lesions is often unusually persistent: Acutely homogeneous and intense persistence has been reported up to 8 days after the intravenous administration of the gadolinium-based contrast material—probably owing to an abnormal retention of the agent by histiocytes (5,20).

In both LCH and non–LCH, patients' T2-weighted MR images may show abnormal symmetric high signal intensity in the dentate nucleus and peridentate regions and their clinical examinations may reveal cerebellar and pyramidal syndromes. Such hyperintense signals have also been reported in the middle cerebellar peduncles in patients with ECD (6,21,22). These lesions do not enhance after contrast material administration and have no mass effect (6,21,22). If the exact origin of these nongranulomatous lesions remains unknown, histologic examination of these dentate nuclei lesions can be performed to reveal extensive loss of myelin sheath tissue, with gliosis and marked sparing of axons (23,24).

Histopathologic analysis plays a key role in differentiating ECD from other types of histiocytosis. ECD differs from LCH in terms of the immunohistologic and microscopic characteristics of the histiocytes, which when associated with ECD are CD68 positive and CD1a negative and do not immunostain for S-100 protein and OKT6. However, these two diseases may coexist, and cases of double infiltration with mixed LCH and ECD have been reported (23,25). In the current study, we observed this phenomenon in one patient, who had symmetric high signal intensity in the dentate and peridentate areas at T2-weighted MR imaging.

Previously reported intraaxial mass lesions in ECD have mainly involved the infratentorial space, including the brain stem, cerebellum, and middle cerebellar peduncles (2). However, these lesions can also be seen in the cerebral hemispheres and the basal ganglia (2,24,26,27) and therefore may be considered ubiquitous, as shown in our series. Intraparenchymal masses in ECD appear rather nonspecific, with a hyperintense or, more frequently, a hypointense signal on T2-weighted MR images and marked enhancement on gadolinium-enhanced MR images. Histopathologic findings are characterized by the accumulation of foamy lipid-laden infiltrating histiocytes with frequent perivascular distribution (23,27).

In our series and other studies, intraorbital lesions were mainly bilateral and limited to the intraconal space (28). At MR imaging, the orbital involvement is visualized as either enhancing well-defined retro-ocular masses sheathing the optic nerves or diffuse infiltration of the retro-ocular fat (28). These intraorbital lesions are clinically evident as exophthalmos or visual impairment, but they also may be asymptomatic, as they were in four patients in the present series, and should be systematically sought, as they are often detected at brain examinations.

An association among multiple lesion locations was the rule in our series. The systemic nature of this non-LCH explains the multiple anatomic sites concomitantly involved. It is interesting that in our series, all of the patients with intracranial lesions also had osteosclerosis of the sinus walls and/or orbital masses. This is of major importance, because in cases of intracranial lesions of uncertain origin, the detection of an associated lesion of the facial bones or orbits at cerebral MR imaging may point to a diagnosis of ECD. Although the association between sinus, orbital, and meningeal lesions also suggests LCH or Wegener granulomatosis (29), both of these diseases are characterized by facial and orbital osteolytic masses.

The main limitation of the current study was the retrospective format. All 33 patients underwent cerebral MR imaging but with different acquisition protocols. Some lesions may have been overlooked, because only 20 of the 33 patients underwent thin-section hypothalamic-pituitary axis MR imaging and 19 underwent dedicated orbital MR imaging exploration. Other limitations were the use of consensus reading rather than independent readings and the lack of interobserver agreement evaluation. Finally, even though we had histologic proof of ECD in each patient, we did not have direct histologic confirmation of each lesion assessed in this work, especially the periarterial and intravenous lesions. The continuity or association of these lesions with other lesions proved to be related to ECD made it highly probable that they had histologic features similar to those of the patients' other lesions that exhibited similar behavior at imaging.

In conclusion, lesions of the brain and meninges, facial bones, and orbits were observed at MR imaging in 91% of the patients with ECD in this study, even those who were free of neurologic symptoms. Therefore, cerebral MR imaging should be performed systematically in this population, because central nervous system involvement can lead to serious disability. Careful attention should also be paid to the periarterial environment and venous compartment. Although the MR findings of individual lesions are nonspecific in ECD, the association among facial bone osteosclerosis, orbital masses, and meningeal or infundibular stalk masses appears to be a cardinal feature of this disease.

Acknowledgment: The authors thank David Seidenwurm, MD, for his assistance in this work.

References

1. Veyssier-Belot C, Cacoub P, Caparros-Lefebvre D, et al. Erdheim-Chester disease: clinical and radiologic characteristics of 59 cases. Medicine (Baltimore) 1996;75(3):157–169.
2. Lachenal F, Cotton F, Desmurs-Clavel H, et al. Neurological manifestations and neuroradiological presentation of Erdheim-Chester disease: report of 6 cases and systematic review of the literature. J Neurol 2006;253(10):1267–1277.
3. Wright RA, Hermann RC, Parisi JE. Neurological manifestations of Erdheim-Chester disease. J Neurol Neurosurg Psychiatry 1999;66(1):72–75.
4. Caparros-Lefebvre D, Pruvo JP, Rémy M, Wallaert B, Petit H. Neuroradiologic aspects of Chester-Erdheim disease. AJNR Am J Neuroradiol 1995;16(4):735–740.

5. Martinez R. Erdheim-Chester disease: MR of intraaxial and extraaxial brain stem lesions. AJNR Am J Neuroradiol 1995; 16(9):1787–1790.

6. Weidauer S, von Stuckrad-Barre S, Dettmann E, Zanella FE, Lanfermann H. Cerebral Erdheim-Chester disease: case report and review of the literature. Neuroradiology 2003;45(4):241–245.

7. Dion E, Graef C, Miquel A, et al. Bone involvement in Erdheim-Chester disease: imaging findings including periostitis and partial epiphyseal involvement. Radiology 2006;238(2):632–639.

8. Gauvrit JY, Oppenheim C, Girot M, et al. Images in cardiovascular medicine: high resolution images obtained with ultrasound and magnetic resonance imaging of pericarotid fibrosis in Erdheim-Chester disease. Circulation 2004;110(15):e443–e444.

9. Haroche J, Amoura Z, Dion E, et al. Cardiovascular involvement, an overlooked feature of Erdheim-Chester disease: report of 6 new cases and a literature review. Medicine (Baltimore) 2004;83(6):371–392.

10. Evidente VG, Adler CH, Giannini C, Conley CR, Parisi JE, Fletcher GP. Erdheim-Chester disease with extensive intraaxial brain stem lesions presenting as a progressive cerebellar syndrome. Mov Disord 1998;13(3):576–581.

11. Boulos AS, Deshaies EM, Qian J, Popp AJ. Preoperative stent placement for intradural vertebral artery stenosis from a rare xanthogranuloma: case report. J Neurosurg 2004; 101(5):864–868.

12. Gazzeri R, Galarza M, Amoroso R, De Bonis C, D'Angelo V. Neurological picture: torcular Erdheim-Chester disease. J Neurol Neurosurg Psychiatry 2006;77(9):1078.

13. Bancroft LW, Berquist TH. Erdheim-Chester disease: radiographic findings in five patients. Skeletal Radiol 1998;27(3):127–132.

14. Marsot-Dupuch K, Le Hir P. Erdheim-Chester disease: a sinonasal lesion mimicking rhinoscleroma. Neuroradiology 2000;42(8):625.

15. Kirchner TH, Seipelt G, Vogl TJ. Involvement of the facial skull in Erdheim-Chester disease [in German]. Rontgenpraxis 2001; 54(4):148–151.

16. Olmos JM, Canga A, Velero C, González-Macías J. Imaging of Erdheim-Chester disease. J Bone Miner Res 2002;17(3):381–383.

17. Albayram S, Kizilkilic O, Zulfikar Z, Islak C, Kocer N. Spinal dural involvement in Erdheim-Chester disease: MRI findings. Neuroradiology 2002;44(12):1004–1007.

18. Curgunlu A, Karter Y, Oztürk A. Erdheim-Chester disease: a rare cause of paraplegia. Eur J Intern Med 2003;14(1):53–55.

19. Johnson MD, Aulino JP, Jagasia M, Mawn LA. Erdheim-chester disease mimicking multiple meningiomas syndrome. AJNR Am J Neuroradiol 2004;25(1):134–137.

20. Tien RD, Brasch RC, Jackson DE, Dillon WP. Cerebral Erdheim-Chester disease: persistent enhancement with Gd-DTPA on MR images. Radiology 1989;172(3):791–792.

21. Fukazawa T, Tsukishima E, Sasaki H, Hamada K, Hamada T, Tashiro K. Erdheim-Chester disease and slowly progressive cerebellar dysfunction. J Neurol Neurosurg Psychiatry 1995;58(2):238–240.

22. Pautas E, Chérin P, Pelletier S, Vidailhet M, Herson S. Cerebral Erdheim-Chester disease: report of two cases with progressive cerebellar syndrome with dentate abnormalities on magnetic resonance imaging. J Neurol Neurosurg Psychiatry 1998;65(4):597–599.

23. Adle-Biassette H, Chetritt J, Bergemer-Fouquet AM, Wechsler J, Mussini JM, Gray F. Pathology of the central nervous system in Chester-Erdheim disease: report of three cases. J Neuropathol Exp Neurol 1997;56(11):1207–1216.

24. Rushing EJ, Kaplan KJ, Mena H, Sandberg GD, Koeller K, Bouffard JP. Erdheim-Chester disease of the brain: cytological features and differential diagnosis of a challenging case. Diagn Cytopathol 2004;31(6):420–422.

25. Vital C, Bioulac-Sage P, Tison F, et al. Brain stem infiltration by mixed Langerhans cell histiocytosis and Chester-Erdheim disease: more than just an isolated case? Clin Exp Pathol 1999;47(2):71–76.

26. Lyders EM, Kaushik S, Perez-Berenguer J, Henry DA. Aggressive and atypical manifestations of Erdheim-Chester disease. Clin Rheumatol 2003;22(6):464–466.

27. Tashjian V, Doppenberg EM, Lyders E, et al. Diagnosis of Erdheim-Chester disease by using computerized tomography-guided stereotactic biopsy of a caudate lesion: case report. J Neurosurg 2004;101(3):521–527.

28. Adem C, Hélie O, Lévêque C, Taillia H, Cordoliani YS. Case 78: Erdheim-Chester disease with central nervous system involvement. Radiology 2005;234(1):111–115.

29. Murphy JM, Gomez-Anson B, Gillard JH, et al. Wegener granulomatosis: MR imaging findings in brain and meninges. Radiology 1999;213(3):794–799.